MULTI-RADAR MULTI-SENSOR (MRMS) SEVERE WEATHER AND AVIATION PRODUCTS

Initial Operating Capabilities

BY TRAVIS M. SMITH, VALLIAPPA LAKSHMANAN, GREGORY J. STUMPF, KIEL L. ORTEGA, KURT HONDL, KAREN COOPER, KRISTIN M. CALHOUN, DARREL M. KINGFIELD, KEVIN L. MANROSS, ROBERT TOOMEY, AND JEFF BROGDEN

The MRMS system's initial operating capabilities for severe weather and aviation include quality-controlled multiradar fields of three-dimensional reflectivity, near-storm environment, and radial velocity derivatives that are used to produce severe weather guidance information.

The Multi-Radar Multi-Sensor (MRMS) system, developed at the National Severe Storms Laboratory and the University of Oklahoma, is now operational at the National Centers for Environmental Prediction (NCEP). The MRMS system consists of the Warning Decision Support System–Integrated Information (WDSS-II; Lakshmanan et al. 2007) suite of severe weather and aviation products and the quantitative precipitation estimation (QPE) products created by the National Mosaic and Multi-Sensor QPE (NMQ; Zhang et al. 2011) system. The MRMS system provides operational guidance for severe convective weather, QPE, and aviation hazards on a seamless three-dimensional grid that is created at a spatial resolution of 0.01° latitude × 0.01° longitude, with 33 vertical levels, every 2 min over the conterminous United States (CONUS) and southern Canada. This paper focuses on the severe weather and aviation set of products that include a three-dimensional (3D) mosaic of reflectivity, guidance for hail, tornado, and lightning hazards, as well as nowcasts of storm location, height, and intensity. MRMS algorithms focusing on quantitative precipitation estimation are discussed in Zhang et al. (2016).

The WDSS-II system (also called MRMS-Severe/Aviation) is a multiradar, multisensor distributed

AFFILIATIONS: SMITH, LAKSHMANAN, ORTEGA, COOPER, CALHOUN, KINGFIELD, TOOMEY, AND BROGDEN—Cooperative Institute for Mesoscale Meteorological Studies, University of Oklahoma, and NOAA/OAR/NSSL, Norman, Oklahoma; STUMPF—Cooperative Institute for Mesoscale Meteorological Studies, University of Oklahoma, Norman, Oklahoma, and NOAA/NWS/MDL, Silver Spring, Maryland; HONDL—NOAA/OAR/NSSL, Norman, Oklahoma; MANROSS—Cooperative Institute for Research in the Atmosphere, University of Colorado Boulder, and NOAA/OAR/ESRL, Boulder, Colorado

CORRESPONDING AUTHOR: Travis Smith, WRDD, NSSL, National Weather Center, 120 David L. Boren Blvd., Norman, OK 73072

E-mail: travis.smith@noaa.gov

The abstract for this article can be found in this issue, following the table of contents.

DOI:10.1175/BAMS-D-14-00173.1

In final form 11 December 2015

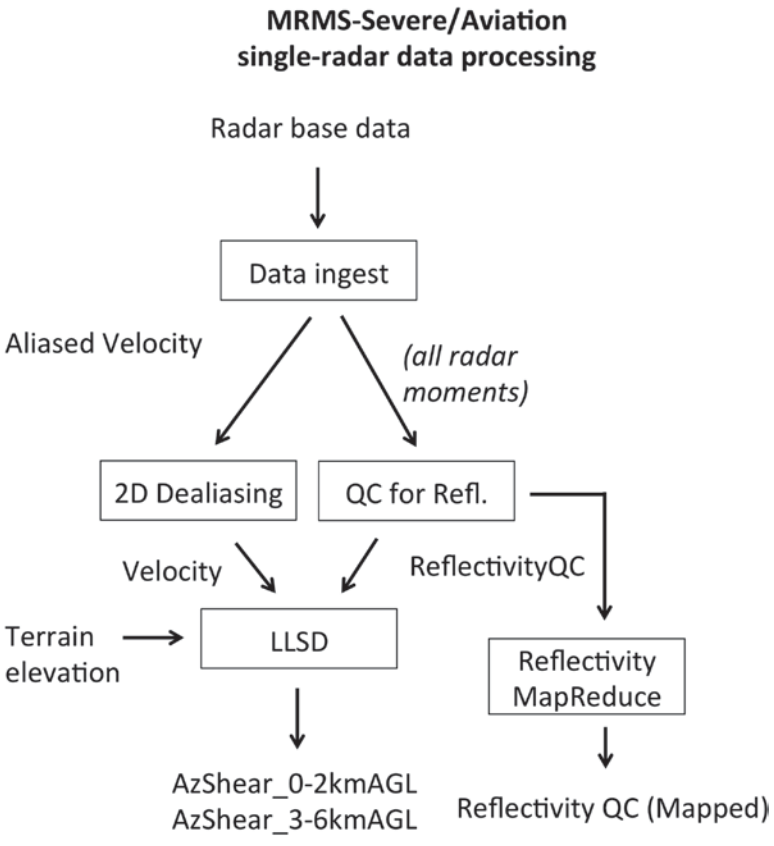

Fig. 1. A simplified data flow diagram for the MRMS-Severe/Aviation single-radar processing. Boxes represent algorithms, while products are listed outside of the boxes.

system that enables the integration of large, disparate datasets into a single seamless, three-dimensional spatial database for analysis by forecasters and is designed for ingest into numerical weather prediction models. Initial inputs into the operational MRMS-Severe/Aviation system include radar data from the U.S. Weather Surveillance Radar-1988 Doppler (WSR-88D) network, the Geostationary Operational Environmental Satellite (GOES) series, surface terrain elevation information, the National Lightning Detection Network (NLDN; Orville 2008), and hourly surface and upper-air analyses from the Rapid Refresh model (Benjamin et al. 2009).

Internally, the MRMS system maintains the data it generates in widely used, self-describing, and extensible data formats, such as Extensible Markup Language (XML) and Network Common Data Form (netCDF; Rew et al. 2015). Some sensors, such as lightning detectors and Doppler radars, provide continuous input data streams, while others, such as satellites or numerical weather prediction models, may update only every 15–60 minutes. The temporal resolution of the various real-time output datasets ranges from 1 minute to hourly updates, while the horizontal spatial resolution is between 0.25 and 100 km^2, depending on the data source. The vertical grid spacing of the three-dimensional radar reflectivity field is irregular, and ranges from 0.25 km near Earth's surface to 1 km at 20 km above mean sea level (MSL).

The motivation behind the MRMS-Severe/Aviation system is the desire to enable forecasters to easily integrate data from multiple sources, whether those sources are several individual radars that sample the same storm from different viewing angles and ranges or satellite, lightning, and other environmental datasets. These data are produced at high resolution on the CONUS scale for processing efficiency, and the various end users may crop this large domain to their area of interest. Many of the end products were created based on field testing with experienced forecasters, who provided valuable ideas for creating this system to help manage their workloads.

SINGLE-RADAR PROCESSING. The first step toward generating MRMS-Severe/Aviation products is the processing of data from individual radars (Fig. 1). These data are received from the National Weather Service (NWS) WSR-88D Level II Central Collection, Distribution and Archive Network in packets of several radials. They are aggregated and handled internally by the system as individual 360° antenna elevation slices (also called a tilt or elevation angle) that were collected as the antenna rotated horizontally. These are, in turn, aggregated into virtual volume scans (Lynn and Lakshmanan 2002) that contain the latest data from every radar elevation tilt in polar coordinates. WSR-88D data are typically 0.5° (azimuthal) by 250-m (range) resolution and have a range of 420 km from the radar site.

On average, each radar samples an elevation slice of the atmosphere every 15–20 s; the central merging system needs to combine the data as they arrive and put them onto a georeferenced 3D grid. In addition, the radar reflectivity data received from the radars do not all consist of hydrometeorological echoes. The echoes could be due to biological returns (such as bats, birds, and insects), anomalous propagation (because of atmospheric conditions, the radar beam may be

reflected downward and may end up showing buildings, roads, and trees, rather than clouds), or such artifacts as sun strobes, terrain occultation, or instrument errors. Therefore, reflectivity data pass through a quality control (QC) neural network (Lakshmanan et al. 2014, 2015) that uses polarimetric variables to eliminate these nonmeteorological radar echoes, producing a field known as reflectivity QC. The data from each tilt is premapped to Cartesian space for later multiradar 3D blending via a MapReduce algorithm (Lakshmanan and Humphrey 2014), which is a technique for handling large datasets via a distributed computing system. Once a tilt of reflectivity data is processed, it is passed on to the multiradar 3D blending algorithm discussed in the next section.

Radial velocity data are quality controlled using the two-dimensional dealiasing method of Jing and Wiener (1993). A linear least squares derivative is computed to calculate the rotational component of the radial velocity field, called azimuthal shear (Smith and Elmore 2004). The calculation of azimuthal shear removes many of the range dependencies (caused by the spreading of the beam as it propagates away from the radar) associated with Doppler radial velocity data and allows the scalar velocity derivatives to be combined from multiple radars. For simplicity in blending azimuthal shear on the CONUS scale, the maximum value of azimuthal shear is computed for two vertical layers once every 2 min: 0–2 and 3–6 km above ground level (AGL). At each tilt, the azimuthal shear values that are not in or near a storm cell (as defined by reflectivity QC greater than or equal to 20 dB*Z* within 5 km of the data point) are removed prior to taking the maximum in each layer at each range. This process preserves high azimuthal shear values that may occur outside of the 20-dB*Z* reflectivity contour, such as in some hook-echo signatures. The 0–2-km AGL azimuthal shear product represents near-surface rotation, while the 3–6-km AGL azimuthal shear product represents rotation in the middle altitudes of a convective storm.

MULTIRADAR BLENDING. Data from 143 WSR-88Ds in the CONUS, as well as 30 radars from Environment Canada (now known as Environment and Climate Change Canada) are blended and mosaicked in real time using the technique described in Lakshmanan et al. (2006b) (Fig. 2). There are several techniques available for 2D and 3D blending, and different techniques are chosen based on the characteristics of the input data fields and the requirements of the end users. An exponential distance-weighted function blends data on the operational system. The CONUS MRMS domain extends from 55°N, 130°W at the northwest corner to 20°N, 60°W at the southeast corner. The domain is updated continuously as new tilts arrive and the output is rewritten every 2 min.

For a 3D grid of radar reflectivity, the initial operating capability of the system interpolates between elevation scans using a spline whose weights are given by a power density function and radars using an exponential distance weighting where observations at a given 3D grid point (or "voxel") are weighted toward data from the nearest radars when multiple radars scan the same location. The horizontal grid spacing is 0.01° latitude × 0.01° longitude (approximately 1-km^2 resolution; 3,500 × 7,000 grid points), with 33 vertical levels from 0 to 20 km MSL for a total of over 800 million voxels. The vertical grid spacing is 250 m from 0 to 3 km MSL, 500 m from 3 to 9 km MSL, and 1000 m from 9 to 20 km MSL. The final product is a 3D volume of quality-controlled reflectivity data that can be used as a stand-alone product or as input into the creation of other data fields.

The two single-radar azimuthal shear layers (0–2 and 3–6 km AGL) are handled as two separate two-dimensional (2D) data fields. The initial operating capability uses the maximum current value from any radar observing a grid point within the previous 5 minutes. The horizontal grid spacing is 0.005° latitude × 0.005° longitude (approximately 0.25-km^2 resolution; 7,000 × 14,000 grid points).

SEVERE WEATHER AND AVIATION PRODUCT GENERATION. The MRMS system runs operationally at the National Oceanic and Atmospheric Administration (NOAA) Integrated Dissemination Program, which is a centralized data dissemination service hosted at NCEP's Central Operations facility in College Park, Maryland, with a backup facility planned in Boulder, Colorado. There are a large number of products generated by the MRMS-Severe/Aviation system, but here we will summarize only those that are distributed on the NOAAPORT (NWS 2015) Satellite Broadcast Network (see the appendix). NOAAPORT distribution provides a one-way broadcast communication of NOAA environmental data and products in near–real time to NOAA at both local National Weather Service forecast offices (NWSFOs) and national centers, as well as to external users. The various end users can subdivide the continental-scale data grids to fit their needs. Figure 2 shows the data flow for generating each set of products. Figure 3 shows a broad view of an example case from the 27 April 2011 tornado outbreak in the southeast United States (Knupp et al. 2014), with Figs. 4–9 showing products at the same time. For brevity, not all products are shown. The "Testing and implementation" section below

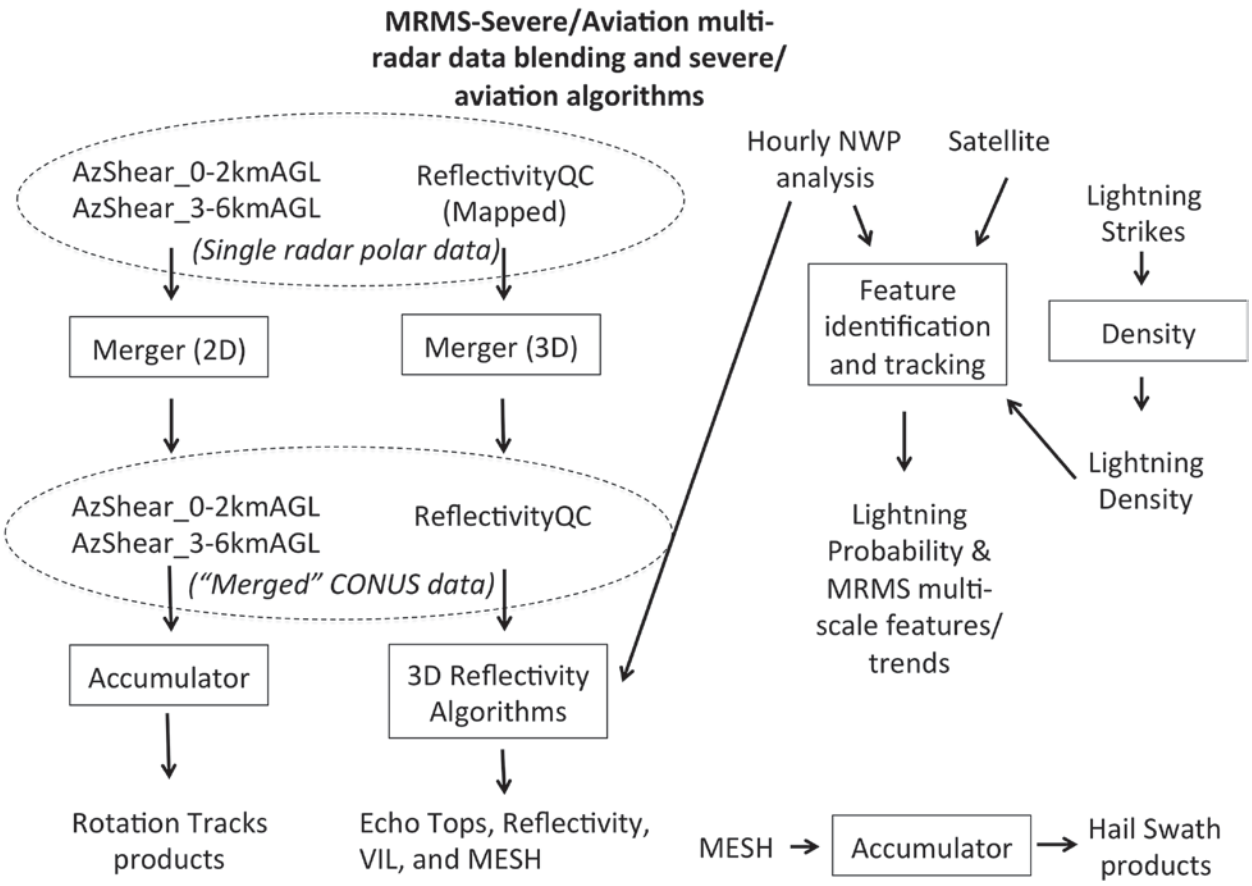

Fig. 2. A data flow diagram for the MRMS-Severe/Aviation multiradar data blending and algorithm processing. Boxes represent algorithms, while a few examples of products and input data are listed outside of the boxes.

describes past field tests at local NWSFOs and in the Hazardous Weather Testbed (HWT) that helped form the basis of how these products may be used.

Reflectivity products. Several radar reflectivity products are generated from the 3D reflectivity field. The three-dimensional nature of the multiradar base reflectivity (Fig. 4) field allows the data to be combined with other 3D data sources and for the creation of multisensor or radar-only derived fields as shown in the next several subsections. The 3D base reflectivity can be converted to flight-level data fields, viewed as integrated vertical layers, or visualized in 3D for aviation use as well (Tait et al. 2015).

Reflectivity at lowest altitude (RALA; Fig. 3) is the reflectivity value closest to Earth's surface. At each grid point, the quality-controlled reflectivity value not influenced by terrain at the lowest elevation is retained. The reflectivity at the lowest altitude may originate from a radar other than the closest radar as a result of terrain beam blockage, especially in the Intermountain West. Weather forecasters use this product as an indication of precipitation intensity near Earth's surface.

Composite reflectivity (Fig. 5, top left) is the maximum value of reflectivity in the vertical column above each grid point. Severe storm and aviation forecasters use this product to view the full horizontal extent of the storm at all altitudes. High-reflectivity features may be observed in this field that may not appear at the lowest altitude or at any one vertical level. A composite reflectivity height product shows the altitude of the reflectivity used for each grid point.

Reflectivities at isotherm levels are the reflectivity values at the 0°, –10°, and –20°C isotherms (Fig. 5, bottom left, top right, and bottom right, respectively), based on the vertical profile of environmental temperature from Rapid Refresh model analysis. Hail growth occurs in the vertical layer between 0° and –20°C, which is usually 2–4 km deep. These products provide weather forecasters a means of identifying intensifying storms that are likely to product hail or lightning in the near future (Tilly et al. 2006).

Echo-top and relative echo-height products. Echo tops are computed using the interpolation technique of Lakshmanan et al. (2013) for 18, 30, 50, and 60 dB*Z*. The

echo-top altitude (Fig. 6) is derived from the 3D merged reflectivity grid. At each grid point, this is the highest altitude in the vertical column where the particular reflectivity value is found (18, 30, 50, or 60 dB*Z*). These products can be useful for quickly identifying rapidly strengthening convection and assessing storm severity. Forecasters use the height of the 50- and 60-dB*Z* echo top as a technique to assess the threat of large hail (Richter and Deslandes 2007). The 18-dB*Z* echo top is used in aviation to determine areas of potentially high turbulence in thunderstorm anvils.

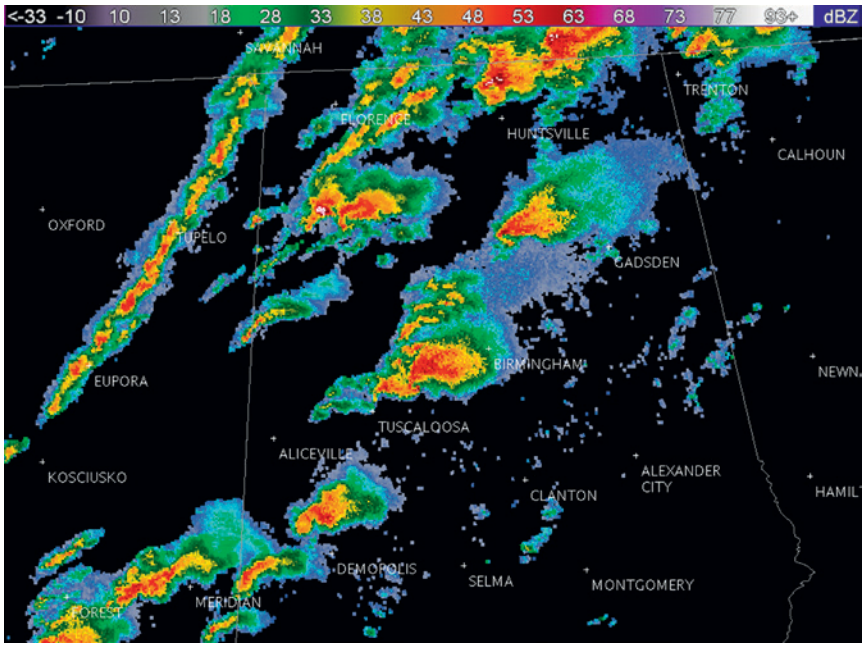

Fig. 3. RALA at 2235 UTC 27 Apr 2015, showing storm cells occurring during a large tornado outbreak in the southeastern United States.

The difference in height between a reflectivity echo-top altitude (50 or 60 dB*Z*) and the altitude of a specific temperature derived from environmental vertical temperature profiles (–20° and 0°C) is calculated by subtracting the height of the given isotherm from the echo top in question. Forecasters use these relative echo heights as another method to estimate the severe hail potential in a thunderstorm (Donavon and Jungbluth 2007). These products can be useful for quickly identifying regions where cloud-to-ground lightning may initiate or become more frequent (MacGorman and Rust 1998). The products produced for the initial operating capabilities of the MRMS system include the height of a 50-dB*Z* echo above –20°C, the height of a 50-dB*Z* echo above 0°C, and the height of a 60-dB*Z* echo above 0°C.

Maximum expected size of hail. The maximum expected size of hail (MESH) product (Fig. 7, left) is an estimate of hail size that is based on the vertical profiles of radar reflectivity and environmental temperature (Witt et al. 1998; Lakshmanan et al. 2006b). MESH is calculated for each horizontal grid point; thus, the data show the spatial extent and hail-size distribution of hail cores within thunderstorms at a given time. Forecasters have made use of the MESH field to provide information to the public about the size of hail to expect via severe thunderstorm warnings (Adrianto et al. 2005).

MESH tracks. The MESH tracks products (Fig. 7, right) show the highest observed MESH value for a specific time period, 60 or 1440 minutes (1 day), at each grid point. The result is a map of areas that were affected by large hail over that time period. Used in real time, MESH tracks show the past path and trends in intensity of the storm and may be used to estimate its direction of movement or to observe changes in direction. Following an event, it may be useful to assess the spatial coverage of potential damage to crops, roofs, and other items that may incur a loss of value when exposed to large hail. It is also useful to operational forecasters during the warning verification process as the product helps narrow the search area for large hail.

Vertically integrated liquid. The vertically integrated liquid (VIL) product (Greene and Clark 1972; Fig. 8) is a measure of liquid water content in a cloud, and high values have frequently been associated with severe weather. It is calculated by integrating the vertical profile of the merged reflectivity above each horizontal grid point and converting it to mass per unit area (kg m^{-2}). Tall storms with high reflectivity values will result in high VIL values; therefore, VIL is one of several products used by forecasters as a general-purpose field to help discriminate between weaker and stronger storms.

Vertically integrated ice. The vertically integrated ice (VII) product (Carey and Rutledge 2000; Mosier et al. 2011) is used to quantify the amount of ice (kg m^{-2}) between the –10° and –40°C isothermal layers. Similar in interpretation to VIL, VII can be used to identify

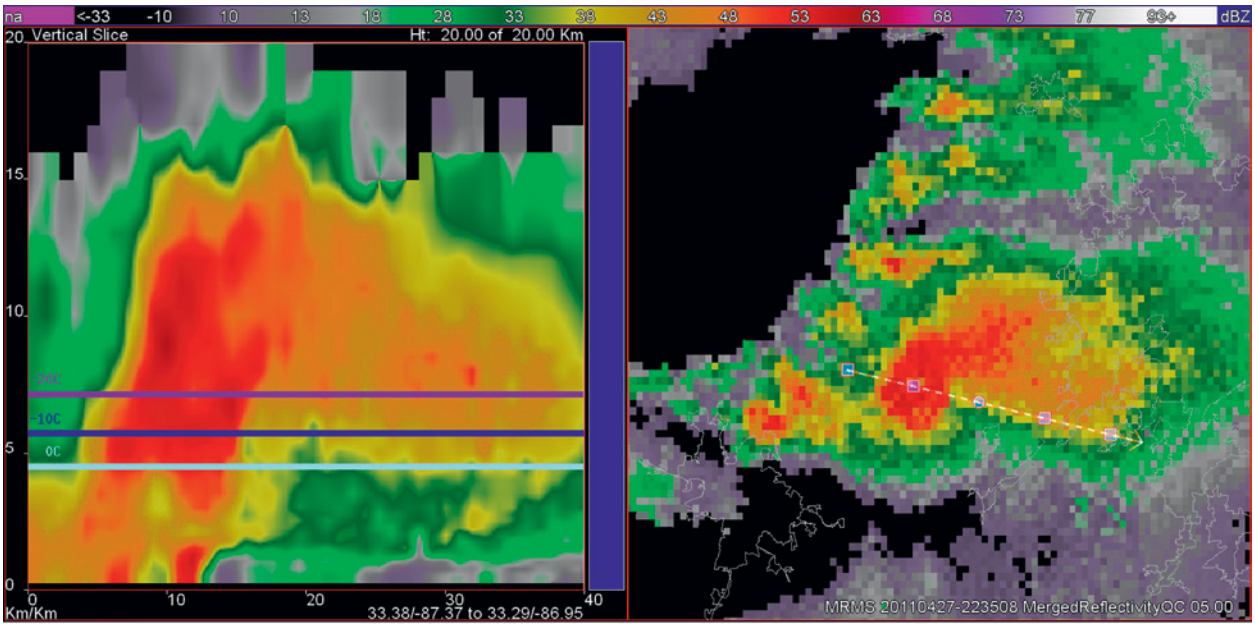

Fig. 4. (left) A vertical cross section of reflectivity from 0 to 20 km MSL along with (right) reflectivity at a constant altitude of 0.5 km MSL showing the 40-km-long cross-sectional location. Aqua, blue, and purple horizontal lines show the altitude of the 0°, −10°, and −20°C isotherms, respectively. This storm was located between Tuscaloosa and Birmingham, AL, at 2235 UTC 27 Apr 2011.

new convective initiation and evaluate changes in updraft intensity. Mosier et al. (2011) used radar-derived VII values to forecast the onset of cloud-to-ground lightning for a 10-yr dataset of summertime thunderstorms near Houston, Texas. The VII method showed improved lead times over other isothermal reflectivity methods; however, additional studies are recommended to evaluate VII's sensitivity across different convective modes, seasons, and geographic regions.

Rotation tracks. A near-surface (0–2 km AGL) azimuthal shear (Fig. 9, left) product highlights circulation patterns and horizontal shear zones in the low altitudes of storms that may be associated with the strong rotation of mesocyclones or tornadic vortex signatures. Strong gust fronts and the leading edges of squall lines can also be identified with the 0–2-km AGL azimuthal shear product. High values (greater than 0.01 s^{-1}) in the midaltitude product (3–6 km AGL) may indicate the presence of a deep mesocyclone, indicative of a well-organized supercell thunderstorm that may have a life cycle of up to several hours. The nonaccumulated azimuthal shear products are not distributed on NOAAPORT as part of the initial operating capability but are used internally as input into other products.

The rotation track products (Fig. 9, right) plot the highest observed azimuthal shear maxima during a specific time interval (60 or 1440 minutes). Two sets of rotation tracks are produced at these two time accumulation intervals, the 0–2-km layer rotation track,and the 3–6-km midaltitude-layer rotation track. This provides a history of the intensity and spatial coverage of strong storm circulation patterns that may be associated with tornadoes or damaging wind.

Lightning density. At every 2D grid point, the lightning density product provides the density of cloud-to-ground lightning flashes that have been recorded at the grid point in the previous 1, 5, 15, or 30 minutes. The grid is smoothed across a 3 × 3 neighborhood. The input data used to generate this field may be obtained from one of several lightning strike data feeds that are commercially available, but for the initial operating capability it is Vaisala's National Lightning Detection Network. Lightning strikes may occur several kilometers from where the core of a storm is identified with radar data, and therefore this information is very useful as a supplementary meteorological dataset to assess the intensity and threat area of storm cells.

Cloud-to-ground lightning probability. At every 2D grid point, the cloud-to-ground (CG) lightning probability product shows the probability of a CG lightning strike in the next 30 minutes. This forecast data field provides guidance to reduce exposure to CG lightning. The algorithm uses radar reflectivity and near-storm environment fields, as well as storm motion estimates

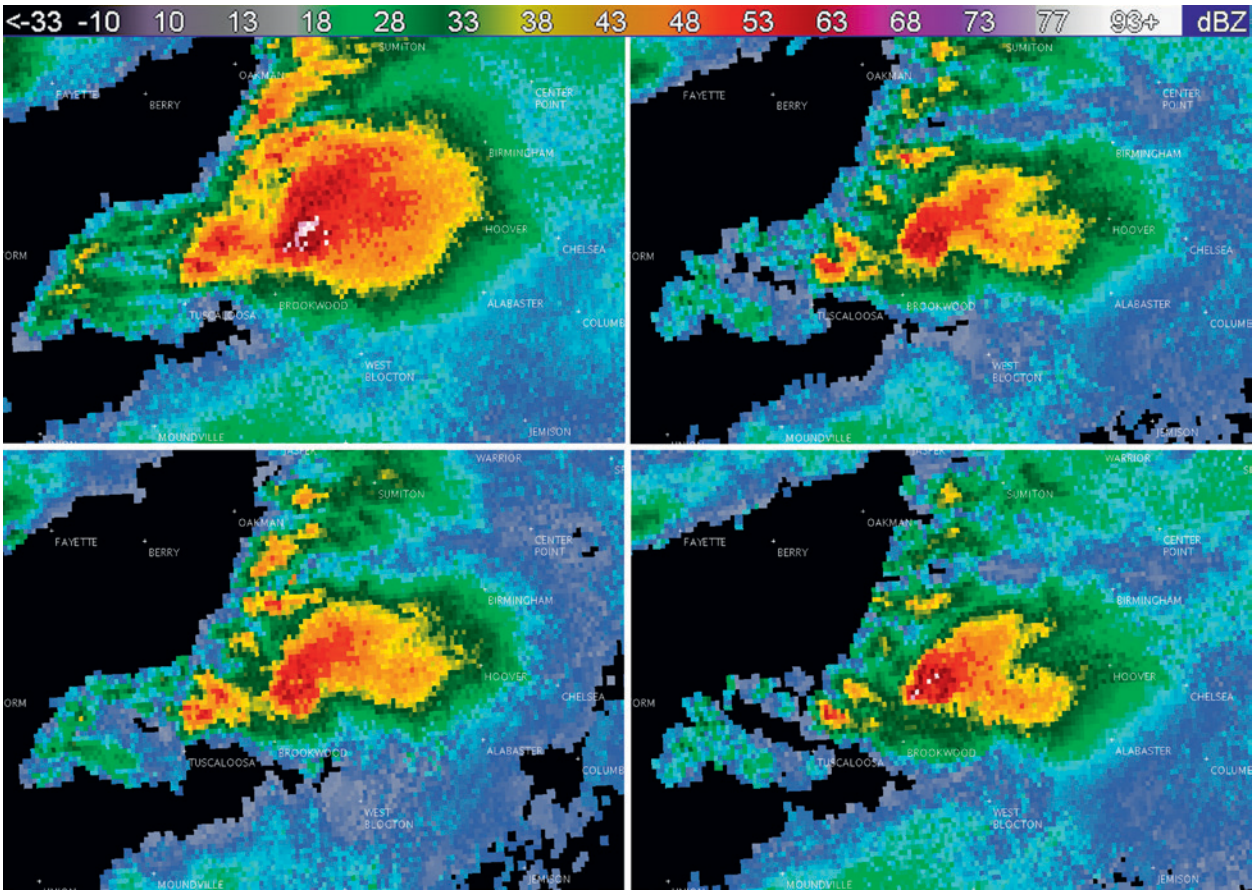

Fig. 5. (top left) Composite reflectivity and reflectivity at isotherm heights of (bottom left) 0°, (top right) −10°, and (bottom right) −20°C for the storm shown in Fig. 4.

as input. The probability is currently computed using a neural network that was trained on historical radar and environmental data from across the United States (Lakshmanan and Smith 2009). However, this guidance is being reprocessed across the CONUS to include in-cloud (IC) lightning density as IC lightning typically precedes CG lightning by 10–30 minutes for a majority of storms (MacGorman et al. 2011). The modifications to and verification of this algorithm will be the subject of a future paper.

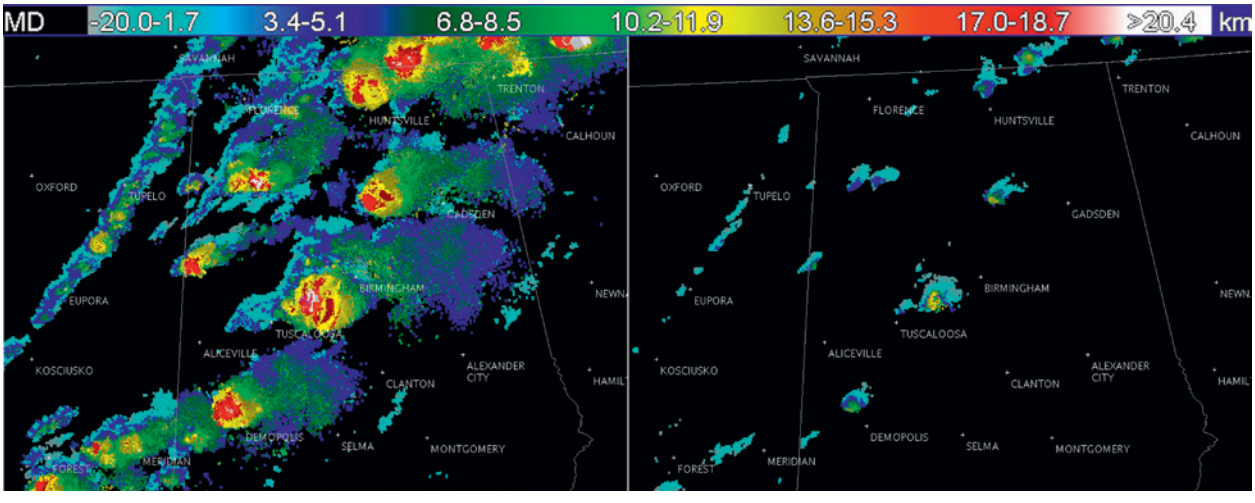

Fig. 6. Echo tops at (left) 18 and (right) 50 dBZ at 2235 UTC 27 Apr 2015. Here, MD indicates areas with no radar echo.

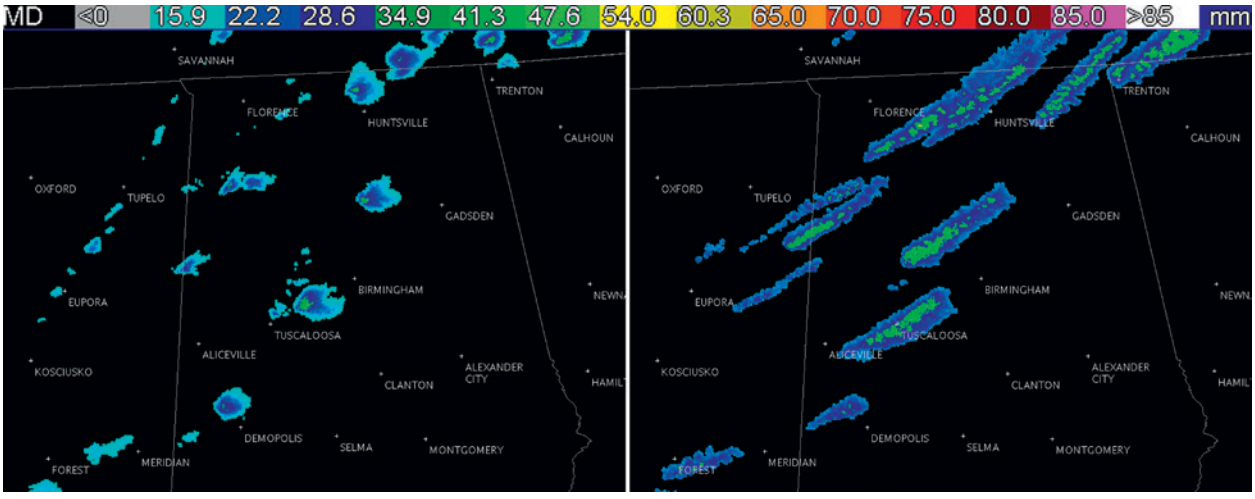

Fig. 7. As in Fig. 3, but for (left) MESH and (right) 1-h MESH tracks.

TESTING AND IMPLEMENTATION. The original Warning Decision Support System (Eilts et al. 1995) was developed as a real-time testing platform for algorithms developed for the WSR-88D system. It received widespread use at NWS forecast offices in the 1990s, but it soon became apparent that a system that was more capable of handling multiple radars and diverse data types was needed to help warning decision-makers manage the ever-increasing flow of data. Hondl (1997) proposed a next-generation WDSS, which was developed in the early 2000s as WDSS-II. An initial WDSS-II MRMS system was installed at the Norman, Oklahoma, NWSFO in 2001 with a second at the Jackson, Mississippi, NWSFO in 2002. Both systems integrated data from multiple nearby WSR-88D radars that cover the county warning area of responsibility for those offices. Similar stand-alone systems were also tested in St. Louis, Missouri, and Wichita, Kansas. WDSS-II had some early success during the Veterans Day tornado outbreak of 9–11 November 2002, with the NWS service assessment of the event stating that "WFO Jackson benefitted from new experimental radar products produced by WDSS-II during the November 10 event" and that its "capabilities should be prioritized for inclusion in future AWIPS [Advanced Weather Interactive Processing System] and future Open Radar Product Generator (ORPG) builds" (NWS 2003, p. 29).

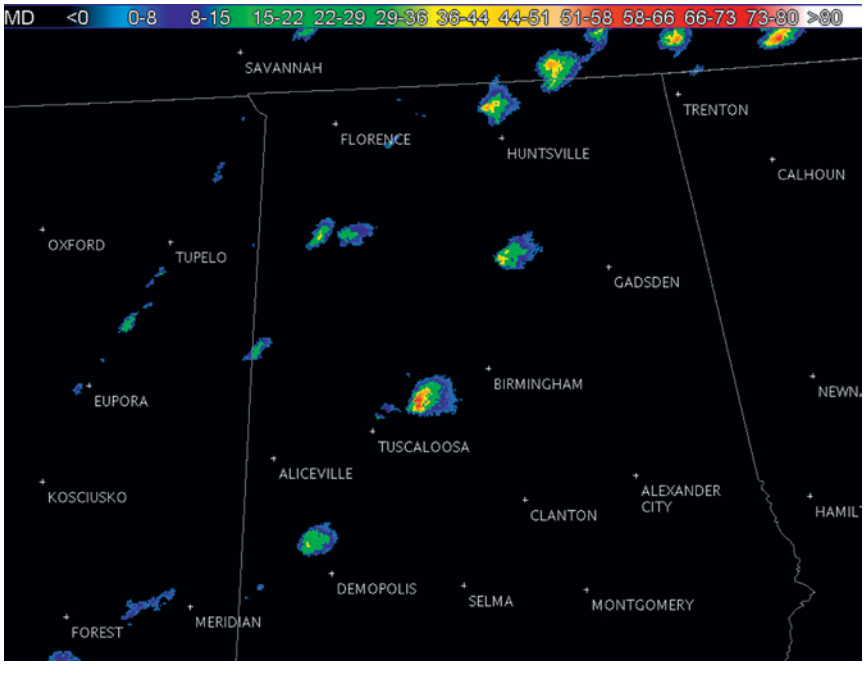

Fig. 8. As in Fig. 3, but for VIL.

The Collaborative Radar Acquisition Field Test (CRAFT; Kelleher et al. 2007) project greatly expanded the distribution capabilities of WSR-88D level II base radar products. By February 2005, a CONUS-wide system was in place (Lakshmanan et al. 2006a) at the National Severe Storms Laboratory (NSSL), and providing guidance to forecasters using the Storm Prediction Center's NCEP Advanced Weather Interactive Processing System (NAWIPS) at 5-min temporal resolution (Levit et al. 2004). Several data fields (hail-size estimates, reflectivity at several

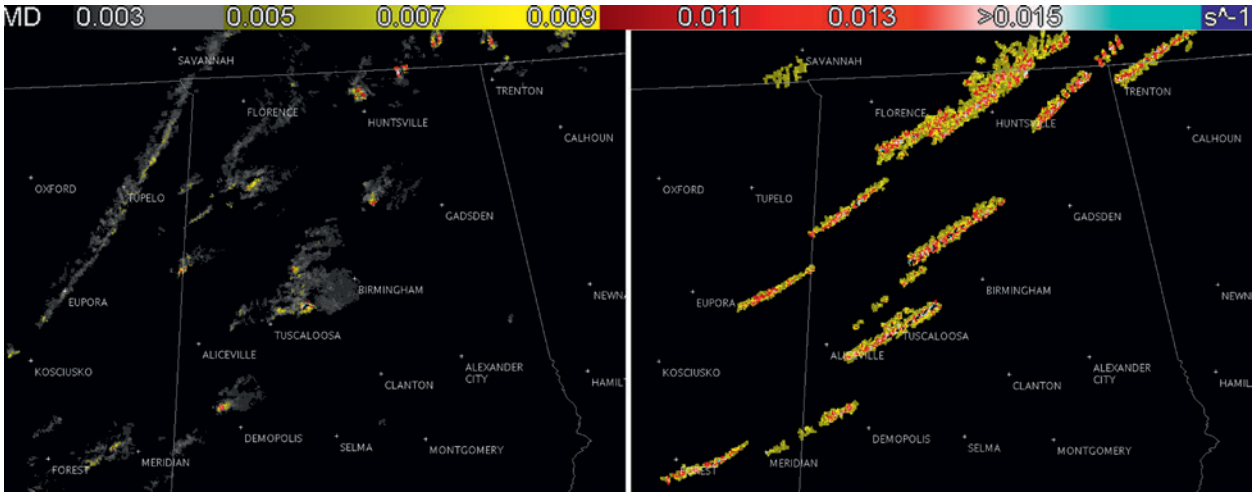

Fig. 9. As in Fig. 3, but for (left) maximum azimuthal shear in the 0–2-km AGL layer and (right) 60-min rotation tracks.

different levels, and rotation tracks) were also supplied in real time to the operational AWIPS at forecast offices in Norman; Fort Worth, Texas; and Tulsa, Oklahoma; for testing and feedback by forecasters to help improve the system.

During 2005, Google introduced the Google Earth virtual globe and Keyhole Markup Language (KML; Google 2015), creating a simple way to distribute geospatial images such as weather radar products (Smith and Lakshmanan 2011). This easy integration of weather radar images with geospatial information such as business locations and phone numbers enabled new high-resolution verification techniques for MRMS severe weather algorithms in the Severe Hazards Analysis and Verification Experiment (SHAVE; Ortega et al. 2009; Fig. 10). Real-time products were also made available online in KML format in 2006 so that anyone could observe the experimental data fields in real time, and a Google Maps interface (http://wdssii.nssl.noaa.gov/maps/) was added in 2008.

The rotation tracks products gained wide use as a first-guess field for providing ground survey crews with guidance in areas that had possible damage following a tornado. Following numerous requests by agencies including the NWS, the Federal Emergency Management Agency, and the American Red Cross, researchers developed the WDSS-II On-Demand interface to automatically generate these data over user-specified time periods for specific geographic areas (Manross et al. 2008). This system was the subject of a NOAA Technology Transfer Award in 2013 for

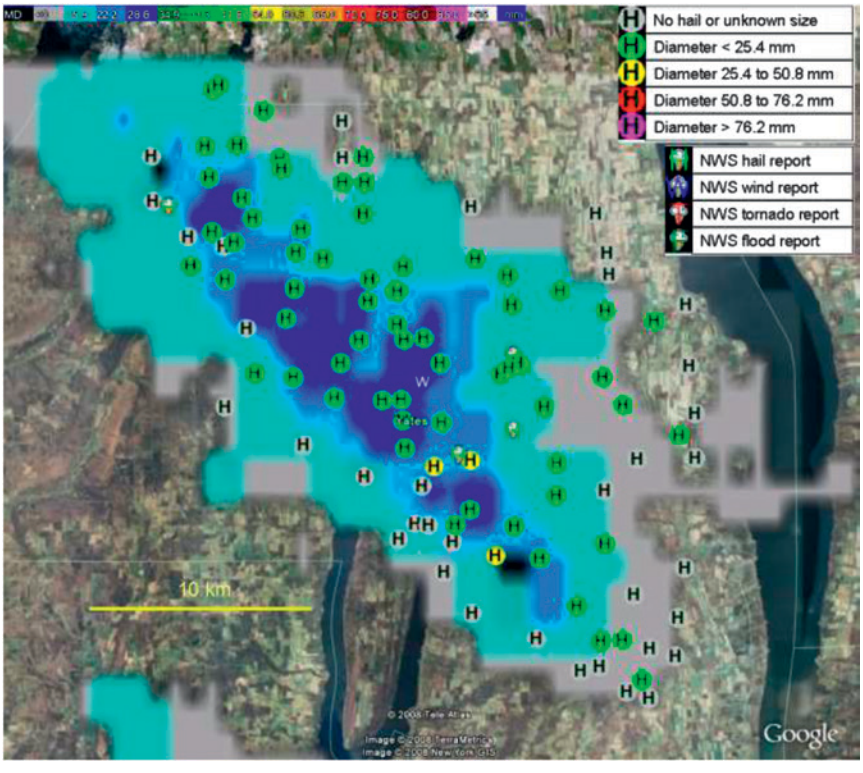

Fig. 10. High-density severe weather reports collected by the SHAVE project on a MESH background displayed in Google Earth.

"the development of an on-demand, near real-time, web-based tool for tracking severe weather and hail swaths across the continental US."

Specific testing of MRMS-Severe/Aviation products occurred in the HWT during 2009 and 2010 (Stumpf et al. 2010). The products were featured in the HWT each following year as well, allowing them to be integrated and tested in the AWIPS and AWIPS2 environments (Kingfield et al. 2013). Forecaster feedback from these real-time experiments helped prioritize which products would be used in the MRMS-Severe/Aviation system when it went operational. Over 250 unique users from the NWS, international agencies, academia, and NOAA research facilities participated in these test activities, many of whom provided direct feedback to improve the MRMS-Severe/Aviation products.

The MRMS-Severe/Aviation system's best practices experiment was conducted during the HWT in 2014, with several goals:

- determine which MRMS products are the most useful for warning decision-making;
- develop optimal AWIPS2 procedures for hail, wind, and tornado warning decision-making;
- determine how MRMS products can be integrated into traditional severe weather diagnosis; and
- suggest new MRMS products and display ideas.

Feedback from NWS forecasters in this and prior experiments led to the development of detailed training modules by the NWS/Warning Decision Training Division (2015) that describe the optimal use of the system for warning decision-making.

MRMS-Severe/Aviation has a wide variety of end users outside of NOAA. Gallo et al. (2012) compared MESH track information to the satellite-based normalized difference vegetation index to identify possible vegetation damage caused by convective storms. Nguy-Robertson et al. (2014) used MRMS hail-size estimates from one wheat-growing season in western Nebraska to help model the threat of the crop-destroying wheat streak mosaic virus during the next growing season. Buler et al. (2012) used MRMS data to estimate bird density in a volume of the atmosphere. Dozens of academic institutions have made use of the software in research, and it has been licensed to various private-sector meteorological companies since 2006 for use in the media and for specific end-user applications.

FUTURE. There are many other key features of the MRMS-Severe/Aviation product suite that are not included in the initial operating capability available on NOAAPORT, but that are likely to be distributed in the future. For instance, storm cell features are identified and tracked using a geospatial image processing technique (Lakshmanan et al. 2003, 2009) that also generates statistics based on various MRMS input fields so that the trends of various storm intensity and environmental parameters may be displayed or collected for analysis. Cintineo et al. (2014) use this algorithm as part of the ProbSevere model, which blends GOES satellite and MRMS radar data to generate probabilistic nowcasts of severe weather occurrence in the next 60 minutes. It is also the basis for automated guidance for probabilistic hazard information being produced as part of the Forecasting a Continuum of Environmental Threats (FACETS; Rothfusz et al. 2014) project and is integral to the GOES-R lightning jump algorithm (Schultz et al. 2009; Chronis et al. 2015). Work is ongoing to integrate MRMS data into Federal Aviation Administration operations (Tait et al. 2015). MRMS-Severe/Aviation applications are used on experimental radars, such as the National Weather Radar Testbed phased array radar in Norman. The system is designed such that adding new data streams usually requires minimal effort.

Some future enhancements incorporate polarimetric radar fields to improve hail-size estimates (Ryzhkov et al. 2013), detect tornado debris signatures (Kingfield et al. 2014; Snyder et al. 2014), and improve reflectivity data quality. Updates to the velocity dealiasing, azimuthal shear calculations, and rotation tracks quality (Miller et al. 2013) are also planned. Additionally, the Multi-Year Reanalysis of Remotely Sensed Storms (MYRORSS; Cintineo et al. 2012; Ortega 2015) project will reprocess all data from the WSR-88D era (1996–present) using MRMS software. MYRORSS will enable data mining of storm attributes, the construction of distributions of MRMS severe weather product values within historical NWS severe weather warnings, and the creation of radar-based severe weather event climatologies. The results of these analyses can be combined to produce real-time hazardous weather event probabilities—a major goal for the FACETs initiative.

SUMMARY. Several individual, automated algorithms have been developed using the MRMS system to yield a forecasting and analysis system that provides real-time products useful in severe weather and aviation nowcasting. Automated algorithms that operate on data from multiple radars can provide information with greater temporal resolution and better spatial coverage than their single-radar counterparts.

MRMS-Severe/Aviation products were developed and tested over a period of more than a decade prior to becoming operational at NCEP. MRMS-Severe/Aviation software integrates knowledge from NWS forecasters, as well as scientific research of storms and their environments, to provide a foundation for managing ever-increasing data flows through intelligent integration of remotely sensed information.

Table ES1. MRMS-Severe/Aviation products that are distributed on the NOAAPORT Satellite Broadcast Network are listed below by official World Meteorological Organization (WMO) header and WMO title.

WMO header	WMO title
YAUC01	Composite reflectivity
YAUC02	Composite reflectivity height
YAUL01	Cloud-to-ground lightning density (1, 5, 15, and 30 min)
YAUL02	Cloud-to-ground lightning probability (0–30 min)
YAUQ01	Base reflectivity
YAUS04	Low-level rotation tracks (60 and 1440 min, accumulated)
YAUS06	Midlevel rotation tracks (60 and 1440 min, accumulated)
YAUS10	Max estimated size of hail (MESH)
YAUS11	MESH tracks (60 and 1440 min, accumulated)
YAUS13	Vertically integrated liquid (VIL)
YAUS15	Vertically integrated ice (VII)
YAUS16	18-, 30-, 50-, and 60-dBZ echo top (ET)
YAUS17	Height of 50-dBZ echo above −20°C
YAUS18	Height of 50-dBZ echo above 0°C
YAUS20	Height of 60-dBZ echo above 0°C
YAUS21	Reflectivity at 0°, −10°, and −20°C
YAUS22	Reflectivity at lowest altitude (RALA)

ACKNOWLEDGMENTS. Funding was provided by the NOAA/Office of Oceanic and Atmospheric Research under NOAA–University of Oklahoma Cooperative Agreement NA11OAR4320072, U.S. Department of Commerce. We wish to thank the hundreds of people who have contributed to the success of this project, including the NSSL information technology, management, and support staff, and the Hazardous Weather Testbed test and evaluation participants. We also wish to thank the editor and anonymous reviews for their excellent comments, which improved the quality of this manuscript.

APPENDIX: MRMS-SEVERE/AVIATION PRODUCTS DISTRIBUTED ON THE NOAAPORT SATELLITE BROADCAST NETWORK. See Table ES1.

REFERENCES

Adrianto, I., T. M. Smith, K. A. Scharfenberg, and T. Trafalis, 2005: Evaluation of various algorithms and display concepts for weather forecasting. Preprints, *21st Int. Conf. on Interactive Information Processing Systems (IIPS) for Meteorology, Oceanography, and Hydrology*, San Diego, CA, Amer. Meteor. Soc., 5.7. [Available online at https://ams.confex.com/ams/Annual2005/techprogram/paper_83928.htm.]

Benjamin, S. G., and Coauthors, 2009: Rapid Refresh/RUC project technical review. NOAA/ESRL/GSD Internal Review. [Available online at http://ruc.noaa.gov/pdf/RR-RUC-TR_11_3_2009.pdf.]

Buler, J., V. Lakshmanan, and D. La Puma, 2012: Improving weather radar data processing for biological research applications: Final report. Technical Report to Patuxtent Wildlife Research Center, USGS, Laurel, MD, 14 pp. [Available online at http://sites.udel.edu/aeroecologyprogram/files/2013/04/FinalReport_w2birddensity.pdf.]

Carey, L. D., and S. A. Rutledge, 2000: The relationship between precipitation and lightning in tropical island convection: A C-band polarimetric study. *Mon. Wea. Rev.*, **128**, 2687–2710, doi:10.1175/1520-0493(2000)128<2687:TRBPAL>2.0.CO;2.

Chronis, T., L. D. Carey, C. J. Schultz, E. V. Schultz, K. M. Calhoun, and S. J. Goodman, 2015: Exploring lightning jump characteristics. *Wea. Forecasting*, **30**, 23–37, doi:10.1175/WAF-D-14-00064.1.

Cintineo, J. L., T. M. Smith, V. Lakshmanan, H. E. Brooks, and K. L. Ortega, 2012: An objective high-resolution hail climatology of the contiguous United States. *Wea. Forecasting*, **27**, 1235–1248, doi:10.1175/WAF-D-11-00151.1.

——, M. J. Pavolonis, J. M. Sieglaff, and D. T. T. Lindsey, 2014: An empirical model for assessing the severe weather potential of developing convection. *Wea. Forecasting*, **29**, 639–653, doi:10.1175/WAF-D-13-00113.1.

Donavon, R. A., and K. A. Jungbluth, 2007: Evaluation of a technique for radar identification of large hail

across the upper Midwest and central plains of the United States. *Wea. Forecasting*, **22**, 244–254, doi:10.1175/WAF1008.1.

Eilts, M. D., J. T. Johnson, E. D. Mitchell, S. Sanger, G. J. Stumpf, and A. Witt, 1995: Warning Decision Support System. Preprints, *11th Conf. on Interactive Information and Processing Systems*, Dallas, TX, Amer. Meteor. Soc., 62–67.

Gallo, K., T. Smith, K. Jungbluth, and P. Schumacher, 2012: Hail swaths observed from satellite data and their relation to radar and surface-based observations: A case study from Iowa in 2009. *Wea. Forecasting*, **27**, 796–802, doi:10.1175/WAF-D-11-00118.1.

Google, 2015: KML reference. [Available online at https://developers.google.com/kml/documentation/kmlreference/.]

Greene, D. R., and R. A. Clark, 1972: Vertically integrated liquid water—A new analysis tool. *Mon. Wea. Rev.*, **100**, 548–552, doi:10.1175/1520-0493(1972)100<0548:VILWNA>2.3.CO;2.

Hondl, K. D., 1997: Warning Decision Support System: The next generation WDSS. Preprints, *28th Conf. on Radar Meteorology*, Austin, TX, Amer. Meteor. Soc., 226–227.

Jing, Z., and G. Wiener, 1993: Two-dimensional dealiasing of Doppler velocities. *J. Atmos. Oceanic Technol.*, **10**, 798–808, doi:10.1175/1520-0426(1993)010<0798:TDDODV>2.0.CO;2.

Kelleher, K., and Coauthors, 2007: Project CRAFT: A real-time delivery system for NEXRAD level II data via the Internet. *Bull. Amer. Meteor. Soc.*, **88**, 1045–1057, doi:10.1175/BAMS-88-7-1045.

Kingfield, D. M., T. Smith, and A. Anderson, 2013: AWIPS-2 in NOAA's Hazardous Weather Testbed: Implementation and display of experimental datasets. *Proc. Third Conf. on Transition of Research to Operations*, Austin, TX, Amer. Meteor. Soc., 441. [Available online at https://ams.confex.com/ams/93Annual/webprogram/Paper217606.html.]

——, S. Degelia, K. L. Ortega, J. C. Snyder, T. M. Smith, and A. V. Ryzhkov, 2014: Development of tornadic debris signature guidance using polarimetric WSR-88D data. *Proc. 27th Conf. on Severe Local Storms*, Madison, WI, Amer. Meteor. Soc., 169. [Available online at https://ams.confex.com/ams/27SLS/webprogram/Paper255252.html.]

Knupp, K. R., and Coauthors, 2014: Meteorological overview of the devastating 27 April 2011 tornado outbreak. *Bull. Amer. Meteor. Soc.*, **95**, 1041–1062, doi:10.1175/BAMS-D-11-00229.1.

Lakshmanan, V., and T. Smith, 2009: Data mining storm attributes from spatial grids. *J. Atmos. Oceanic Technol.*, **26**, 2353–2365, doi:10.1175/2009JTECHA1257.1.

——, and T. W. Humphrey, 2014: A MapReduce technique to mosaic continental-scale weather radar data in real-time. *IEEE J. Sel. Top. Appl. Earth Obs. Remote Sens.*, **7**, 721–732, doi:10.1109/JSTARS.2013.2282040.

——, R. Rabin, and V. DeBrunner, 2003: Multiscale storm identification and forecast. *Atmos. Res.*, **67–68**, 367–380, doi:10.1016/S0169-8095(03)00068-1.

——, T. M. Smith, K. Cooper, J. J. Levit, G. J. Stumpf, and D. R. Bright, 2006a: High-resolution radar data and products over the continental United States. Preprints, *22nd Conf. on Interactive Information Processing Systems*, Atlanta, GA, Amer. Meteor. Soc., 9.7. [Available online at https://ams.confex.com/ams/Annual2006/techprogram/paper_103054.htm.]

——, ——, K. Hondl, G. J. Stumpf, and A. Witt, 2006b: A real-time, three-dimensional, rapidly updating, heterogeneous radar merger technique for reflectivity, velocity, and derived products. *Wea. Forecasting*, **21**, 802–823, doi:10.1175/WAF942.1.

——, ——, G. J. Stumpf, and K. D. Hondl, 2007: The Warning Decision Support System—Integrated Information. *Wea. Forecasting*, **22**, 596–612, doi:10.1175/WAF1009.1.

——, K. Hondl, and R. Rabin, 2009: An efficient, general-purpose technique for identifying storm cells in geospatial images. *J. Atmos. Oceanic Technol.*, **26**, 523–537, doi:10.1175/2008JTECHA1153.1.

——, ——, C. K. Potvin, and D. Preignitz, 2013: An improved method for estimating radar echo-top height. *Wea. Forecasting*, **28**, 481–488, doi:10.1175/WAF-D-12-00084.1.

——, C. Karstens, J. Krause, and L. Tang, 2014: Quality control of weather radar data using polarimetric variables. *J. Atmos. Oceanic Technol.*, **31**, 1234–1249, doi:10.1175/JTECH-D-13-00073.1.

——, ——, ——, K. Elmore, A. Ryzhkov, and S. Berkseth, 2015: Which polarimetric variables are important for weather/no-weather discrimination? *J. Atmos. Oceanic Technol.*, **32**, 1209–1223, doi:10.1175/JTECH-D-13-00205.1.

Levit, J. J., V. Lakshmanan, K. Manross, and R. S. Schneider, 2004: Integration of the Warning Decision Support System—Integrated information into the NOAA Storm Prediction Center. Preprints, *22nd Conf. on Severe Local Storms*, Hyannis, MA, Amer. Meteor. Soc., 8B.4. [Available online at https://ams.confex.com/ams/11aram22sls/techprogram/paper_81821.htm.]

Lynn, R. J., and V. Lakshmanan, 2002, Virtual radar volumes: Creation, algorithm access and visualization. Preprints, *21st Conf. on Severe Local Storms*, San

Antonio, TX, Amer. Meteor. Soc., P5.3. [Available online at https://ams.confex.com/ams/pdfpapers/47546.pdf.]

MacGorman, D. R., and W. D. Rust, 1998: *The Electrical Nature of Storms.* Oxford Press, 422 pp.

——, I. R. Apostolakopoulos, N. R. Lund, N. W. S. Demetriades, M. J. Murphy, and P. R. Krehbiel, 2011: The timing of cloud-to-ground lightning relative to total lightning activity. *Mon. Wea. Rev.*, **139**, 3871–3886, doi:10.1175/MWR-D-11-00047.1.

Manross, K. L., T. M. Smith, J. T. Ferree, and G. J. Stumpf, 2008: An on-demand user interface for requesting multi-radar, multi-sensor time accumulated products to support severe weather verification. *23rd Conf. on Interactive Information Processing Systems*, New Orleans, Amer. Meteo. Soc., P2.13. [Available online at https://ams.confex.com/ams/pdfpapers/134621.pdf.]

Miller, M. L., V. Lakshmanan, and T. Smith, 2013: An automated method for depicting mesocyclone paths and intensities. *Wea. Forecasting*, **28**, 570–585, doi:10.1175/WAF-D-12-00065.1.

Mosier, R. M., C. Schumacher, R. E. Orville, and L. D. Carey, 2011: Radar nowcasting of cloud-to-ground lighting over Houston, Texas. *Wea. Forecasting*, **26**, 199–212, doi:10.1175/2010WAF2222431.1.

Nguy-Robertson, A. L., A. Stilwell, A. I. Zygielbaum, J. McMechan, G. Hein, S. Wegulo, and T Smith, 2014: Developing the framework for a risk map for mite-vectored viruses in wheat resulting from pre-harvest hail damage. *2014 Fall Meeting*, San Francisco, CA, Amer. Geophys. Union, Abstract B51I-0123.

NWS, 2003: Veterans Day weekend tornado outbreak of November 9-11, 2002. NWS Service Assessment, 37 pp. + appendixes. [Available online at www.nws.noaa.gov/os/assessments/pdfs/veteran.pdf.]

——, 2015: NOAAPORT user's page. [Available online at www.nws.noaa.gov/noaaport/html/noaaport.shtml.]

NWS/Warning Decision Training Division, 2015: Multi-Radar/Multi-Sensor information and training. [Available online at www.wdtb.noaa.gov/courses/MRMS/.]

Ortega, K. L., 2015: A radar-based storm climatology for the contiguous United States for improved severe weather climatologies and warnings. *Proc. 31st Conf. on Environmental Information Processing Technologies*, Phoenix, AZ, Amer. Meteor. Soc., 10.3. [Available online at https://ams.confex.com/ams/95Annual/webprogram/Paper262017.html.]

——, T. M. Smith, K. L. Manross, K. A. Scharfenberg, A. Witt, A. G. Kolodziej, and J. J. Gourley, 2009: The Severe Hazards Analysis and Verification Experiment. *Bull. Amer. Meteor. Soc.*, **90**, 1519–1530, doi:10.1175/2009BAMS2815.1.

Orville, R. E., 2008: Development of the National Lightning Detection Network. *Bull. Amer. Meteor. Soc.*, **89**, 180–190, doi:10.1175/BAMS-89-2-180.

Rew, R. K., G. P. Davis, S. Emmerson, and H. Davies, 2015: NetCDF user's guide for C: An interface for data access. Unidata, UCAR. [Available online at www.unidata.ucar.edu/software/netcdf/guide_toc.html.]

Richter, H., and R. B. Deslandes, 2007: The four large hail assessment techniques in severe thunderstorm warning operations in Australia. Preprints, *33rd Conf. on Radar Meteorology*, Cairns, QLD, Australia, Amer. Meteor. Soc., P5.19. [Available online at https://ams.confex.com/ams/pdfpapers/123766.pdf.]

Rothfusz, L., C. D. Karstens, and D. Hilderbrand, 2014: Forecasting a continuum of environmental threats: Exploring next-generation forecasting of high impact weather. *Eos, Trans. Amer. Geophys. Union*, **95**, 325–326, doi:10.1002/2014EO360001.

Ryzhkov, A. V., M. R. Kumjian, S. M. Ganson, and P. Zhang, 2013: Polarimetric radar characteristics of melting hail. Part II: Practical implications. *J. Appl. Meteor. Climatol.*, **52**, 2871–2886, doi:10.1175/JAMC-D-13-074.1.

Schultz, C. J., W. A. Petersen, and L. D. Carey, 2009: Preliminary development and evaluation of lightning jump algorithms for the real-time detection of severe weather. *J. App. Meteor. Climatol.*, **48**, 2543–2563, doi:10.1175/2009JAMC2237.1.

Smith, T. M., and K. L. Elmore, 2004: The use of radial velocity derivatives to diagnose rotation and divergence. Preprints, *11th Conf. on Aviation, Range, and Aerospace*, Hyannis, MA, Amer. Meteor. Soc., P5.6. [Available online at https://ams.confex.com/ams/pdfpapers/81827.pdf.]

——, and V. Lakshmanan, 2011: Real-time, rapidly updating severe weather products for virtual globes. *Comput. Geosci.*, **37**, 3–12, doi:10.1016/j.cageo.2010.03.023.

Snyder, J. C., A. V. Ryzhkov, D. M. Kingfield, S. Degelia, and K. L. Ortega, 2014: Implementation of tornadic debris signature guidance using polarimetric WSR-88D data. *Proc. 27th Conf. on Severe Local Storms*, Madison, WI, Amer. Meteor. Soc., 75. [Available online at https://ams.confex.com/ams/27SLS/webprogram/Paper255954.html.]

Stumpf, G. J., B. C. Baranowski, D. M. Kingfield, K. M. Kuhlman, K. L. Manross, C. W. Siewert, T. M. Smith, and S. Stough, 2010: Real-time severe convective weather warning exercises at the Experimental Warning Program 2010 (EWP2010). *Proc. 25th Conf. on Severe Local Storms*, Denver, CO, Amer. Meteor. Soc., 7B.2. [Available online at https://ams.confex.com/ams/25SLS/techprogram/paper_176208.htm.]

Tait, C., V. Passetti, and S. Abelman, 2015: Federal Aviation Administration Multi-Radar Multi-Sensor System research to operations accomplishments. *Proc. 17th Conf. on Aviation, Range, and Aerospace Meteorology*, Phoenix, AZ, Amer. Meteor. Soc., 312. [Available online at https://ams.confex.com/ams/95Annual/webprogram/Paper258567.html.]

Tilly, D., R. W. Przybylinski, and T. M. Smith, 2006: Overview of the 2005 and spring 2006 WDSS-II demonstration at WFO St. Louis. Preprints, *23rd Conf. on Severe Local Storms*, St. Louis, MO, Amer. Meteor. Soc., P5.2. [Available online at https://ams.confex.com/ams/pdfpapers/115487.pdf.]

Witt, A., M. D. Eilts, G. J. Stumpf, J. T. Johnson, E. D. Mitchell, and K. W. Thomas, 1998: An enhanced hail detection algorithm for the WSR-88D. *Wea. Forecasting*, **13**, 286–303, doi:10.1175/1520-0434(1998)013<0286:AEHDAF>2.0.CO;2.

Zhang, J., and Coauthors, 2011: National Mosaic and Multi-Sensor QPE (NMQ) system: Description, results, and future plans. *Bull. Amer. Meteor. Soc.*, **92**, 1321–1338, doi:10.1175/2011BAMS-D-11-00047.1.

——, and Coauthors, 2016: Multi-Radar Multi-Sensor (MRMS) quantitative precipitation estimation: Initial operating capabilities. *Bull. Amer. Meteor. Soc.*, **97**, 621–637, doi:10.1175/BAMS-D-14-00174.1.